Composites Science and Technology, **47**, 321-329 (1992)

On the Phenomenon of Curved Microcracks in $[(S)/90_n]_S$ Laminates: Their Shapes, Initiation Angles, and Locations

Shoufeng Hu, Jong S. Bark, and John A. Nairn

Materials Science and Engineering, University of Utah, Salt Lake City, Utah 84112

ABSTRACT

A variational analysis for the stress state in microcracked cross-ply laminates was used to investigate the phenomenon of curved microcracking in $[(S)/90_n]_S$ laminates. Previous investigators proposed that the initiation and orientation of curved microcracks are controlled by local maxima and stress trajectories of the principal stresses. We implemented a principal stress model using a variational mechanics stress analysis and we were able to make predictions about curved microcracks. The predictions agree well with experimental observations and therefore support the assertion that the variational analysis gives an accurate stress state that is useful for modeling the microcracking properties of cross-ply laminates. An important prediction about curved microcracks is that they are a late stage of microcracking damage. They only occur when the crack density of straight microcracks exceeds some critical value — the critical crack density for curved microcracking. The predicted critical crack density for curved microcracking agrees well with experimental observations.

Key words: *Microcracking, Curved Microcracks, Variational Analysis, Fracture,Cross-Ply Laminates*

INTRODUCTION

Matrix microcracking in the off-axis plies of $[(S)/90_n]_s$ laminates, where (S) is any non-90˚-ply orthotropic sublaminate, has been the subject of extensive investigations for many years. Most work concentrates on the phenomenon of straight microcracks in the 90˚ plies. The goal is typically to predict the straight microcrack density as a function of applied load and the effect of those microcracks on the longitudinal stiffness. Several analytical models, including one-dimensional or two-dimensional shear-lag models[1-5] and a variational analysis model,[6,7] have been proposed. A recent review presents strong arguments that the variational analysis model is superior to the other models.[8] First, the variational analysis agrees well with many experimental observations. Second, the variational analysis is unique in its ability to distinguish the microcracking properties of $[(S)/90_n]_s$ laminates from those of $[90_n/(S)]_n$ laminates. It can do so because it includes the thickness direction stresses that are ignored by other analyses (*e.g.*, Refs. [1-5]). Inclusion of the thickness direction stresses is essential for analyzing curved microcracks as well. In contrast to shear-lag models,[1-5] therefore, the variational analysis model[6,7] has the potential of explaining and analyzing the phenomenon of curved microcracking.

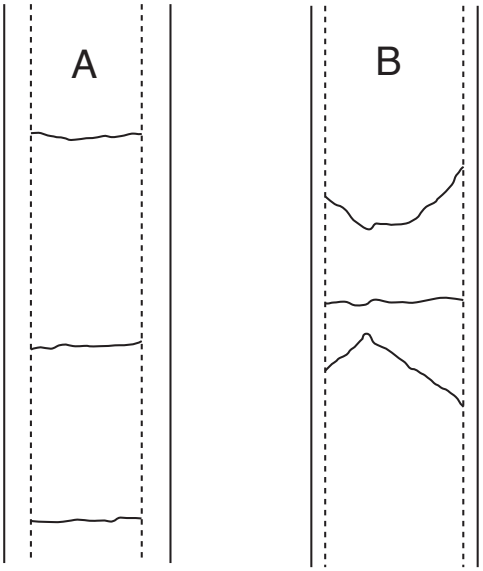

Figure 1: Sketches of actual edge view of typically damaged $[(S)/90_n]_S$ laminates. A. Roughly periodic array of straight microcracks in a AS4/PEEK $[0/90_4]_S$ laminate. B. Two curved microcracks near one straight microcrack in a AS4/PEEK $[0/90_8]_S$ laminates.

Several researchers[9-11] have reported observing curved microcracks in cross-ply laminates. A typical curved microcrack observed from the edge of the laminate is shown in Fig. 1B. The curved microcrack is always located near an existing straight microcrack. It initiates at the 0/90 interface making an angle of 40°-60° with respect to the interface. At early stages of microcracking the failure process is dominated by straight microcracking (see Fig. 1A); at late stages of microcracking, curved microcracking begins and it eventually dominates the failure process.[9-11] One consequence of curved microcracks is a reduction in longitudinal stiffness. Allen *et. al.*[12] point out that curved microcracks reduce the out-of-plane as well as the in-plane stiffnesses.

Most investigations on curved microcracks are limited to a description of the experimental phenomena and to suppositions of their possible reasons. Groves *et. al.*[11] present the only attempt at understanding the mechanism behind curved microcracks. Their analysis is based on two assumptions:

1. The locations of local maxima in the principal stresses determine the locations for the initiation of curved microcracks.

2. The crack runs normal to the larger or first principal stress and thus the microcrack trajectory is determined by the trajectory of the second principal stress.

They use these two assumptions and finite element analysis to predict the formation of curved microcracks and find satisfactory agreement with experimental results.

If an analytical stress state is used with the above two assumptions, it is possible to make analytical predictions about the formation of curved microcracks. If the analytical predictions agree with experimental results then we have new tools that are considerably easier to use and perhaps more general than finite element analysis techniques. Perhaps more significantly, successful analytical methods will indicate that the stress state used in deriving the predictions accurately represents the distribution of principal stresses. Verified analyses that result in accurate stress states are essential to fundamental understanding of composite failure processes. In the present study, we used the analytical stress state provided by Hashin's variational analysis.[6,7] Using Groves *et. al.*[11] two assumptions we made predictions for the locations and orientations of curved microcracks. The predictions agree well with experimental observations. Using Groves *et. al.*[11] second assumption, we calculated the predicted shapes of curved microcracks. The predicted shapes qualitatively agree with observed curved microcrack shapes. The analysis led us to define a critical crack density for curved microcracking. Below the critical crack density only straight microcracks are observed; above the critical crack density new microcracks are predominantly curved microcracks.

MATERIALS AND METHODS

Hercules AS4 carbon/poly-ether-ether-ketone (AS4/PEEK) and Hercules AS4 carbon/3501-6 epoxy (AS4/3501-6) composite specimens were provided by ICI Composites, Inc. and by Hercules, Inc., respectively. The AS4/PEEK specimens were supplied as laminated composites. The AS4/3501-6 specimens were provided in prepreg form. We autoclave cured the AS4/3501-6 specimens according to manufacturer's recommendations. Cross-ply laminates of generic layup $[(S)/90_n]_s$ and $[90_n/(S)]_s$ were tested in tension on a 5 kN MTS testing machine. The nomenclature (S) means any non-90°-ply orthotropic sublaminate. Our results were confined to (S) of $[0_n]$ or $[\pm\theta]$ where θ=15° or 30°. The specimens were 12.7 mm (width) by 90±10 mm or 68±3 mm (effective length) for AS4/PEEK or AS4/3501-6, respectively. The single ply thicknesses for both materials were 0.154 mm. The total specimen thicknesses ranged from 0.61 mm to 2.77 mm.

The testing machine was equipped with an IBM personal computer for data recording and processing. A uniaxial load was applied through aluminum end tabs glued to the specimens and gripped with serrated-type faces in hydraulic grips. A 50 mm extensometer was mechanically attached to the specimen to measure displacements during testing. The loading was interrupted periodically to measure the axial stiffness and to document the damage state by examining the microcracks using optical microscopy. $[(S)/90_n]_s$ laminates were examined on the edges. $[90_n/(S)]_s$ laminates were examined both on the edges and on the faces.

The unidirectional material constants for these materials are given below. The 1-2-3 directions correspond to the fiber, transverse, and thickness directions.

AS4/PEEK:

$E_1 = 130.0$ GPa $\quad E_2 = 9.7$ GPa $\quad G_{12} = 5.5$ GPa

$G_{23} = 2.6$ GPa $\quad \nu_{12} = 0.3$ $\quad \nu_{23} = 0.35$

AS4/3506-1:

$E_1 = 130.0$ GPa $\quad E_2 = 9.7$ GPa $\quad G_{12} = 5.0$ GPa

$G_{23} = 3.6$ GPa $\quad \nu_{12} = 0.3$ $\quad \nu_{23} = 0.5$

EXPERIMENTAL OBSERVATIONS

The original purpose of the testing was to study the general microcracking properties of AS4/PEEK and AS4/3501-6 laminates. The results were expected and were found to be dominated by straight microcracking. Some laminates, however, showed curved microcracks. The observation and analysis of the curved microcracks are a by-product of the larger microcracking study. We tested eight different laminate structures for AS4/PEEK, of which three laminates had 90˚ plies in the middle ($[(S)/90_n]_s$) and five had 90˚ plies on the surfaces ($[90_n/(S)]_s$). We tested twenty one different laminate structures for AS4/3501-6, of which ten laminates had 90˚ plies in the middle and eleven had 90˚ plies on the surfaces. For each laminate structure we typically tested three replicate specimens.

Curved microcracks were only observed in laminates having 90˚ plies in the middle ($[(S)/90_n]_s$). No curved microcracks were found in any of the $[90_n/(S)]_n$ laminates. The remainder of this paper, therefore, will be confined to $[(S)/90_n]_s$ laminates. Curved microcracks in $[(S)/90_n]_s$ laminates were always observed to initiate at the 0/90 interface. The initial trajectories of the curved microcracks made angles of 40˚–60˚ with respect to the 0/90 interface. A tracing of two typical curved microcracks is shown in Fig. 1B. As the thickness of the 90˚ ply group increased, the strain to initiate curved microcracks decreased. Likewise, decreasing the stiffness of the [(S)] sublaminate reduced the strain to initiate curved microcracking.

In contrast to straight microcracks which typically grow rapidly across the cross-section of the 90˚ ply group[8], curved microcracks appear to start at the ply interface and grow slowly across the 90˚ ply group. X-ray radiographs in Ref. [11] confirm the slow growth nature of curved microcracks. Our experimental observations as well as the results in Ref. [11] show that curved microcracks are sometimes single-sided cracks that originate at one ply interface but never grow across the entire thickness of the 90˚ ply group. These single-sided cracks have sometimes been termed oblique microcracks.[9,10] It is possible for two single-sided cracks to begin near the same straight microcrack but on opposite sides of the 90˚ ply group. Such pairs of microcracks have a tendency to grow towards each other, but they may not always coalesce at the center to form a

complete curved microcrack. As stated previously, curved microcracks are always associated with and located near existing straight microcracks. A given straight microcrack may be associated with zero, one, or two curved microcracks — all these possibilities were observed. In our analysis we found that the location of curved microcracks relative to the existing straight microcrack and whether or not it will even form are determined by the distance from the straight microcrack to the next straight microcrack. In other words, the curved microcrack formation process is determined by the size of the straight microcrack interval in which the curved microcrack forms. Because the two microcrack intervals above and below each straight microcrack may be of different size, the curved microcracks above or below each straight microcrack may appear at different locations, or may not appear at all.

Experimental observations indicated that more delaminations initiated from the tips of curved microcracks than from the tips of straight microcracks. In Ref. [13] a new variational analysis is developed and used to make predictions about delaminations emanating from straight microcrack tips in $[(S)/90_n]_s$ and $[90_n/(S)]_n$ laminates. One important prediction is that local compression effects at the tips of straight microcracks in $[(S)/90_n]_s$ laminates inhibits the delamination process. This predicted inhibition agrees with our experimental observations on straight microcracks. The stress state at the tips of curved microcracks, however, is apparently different. It promotes delaminations. The ability of curved microcracks to nucleate further damage in composite laminates increases the importance of understanding the conditions under which they form.

THEORETICAL PREDICTIONS

The variational stress analysis, originally developed by Hashin, provides an approximate stress state for the unit cell of damage in a typical $[(S)/90_n]_s$ laminate (see Refs. [6] and [7]). The unit cell of damage, illustrated in Fig. 2, is the region bounded by two straight microcracks. A coordinate system is introduced such that the x, y, and z axes are in the longitudinal, width and thickness directions of the laminate, respectively. The origin is at the center of the specimen. The approximate stress state in the 90˚ plies is written as:

$$\sigma_{xx}^{(1)} = \sigma_{x0}^{(1)} - \psi(x) \qquad \tau_{xz}^{(1)} = \psi'(x)z \qquad \sigma_{zz}^{(1)} = \psi''(x)(ht_1 - z^2)/2 \tag{1}$$

where superscript (1) and subscript 1 denote quantities for the 90˚ plies, h is the half thickness of the laminate, $\sigma_{x0}^{(1)}$ is the normal stress in the 90˚ plies prior to formation of any microcracks, and $\psi(x)$ is an unknown function of x. $\psi(x)$ can be determined analytically by minimizing of the total complementary energy. The reader is referred to Refs. [6] and [7] for details and for the

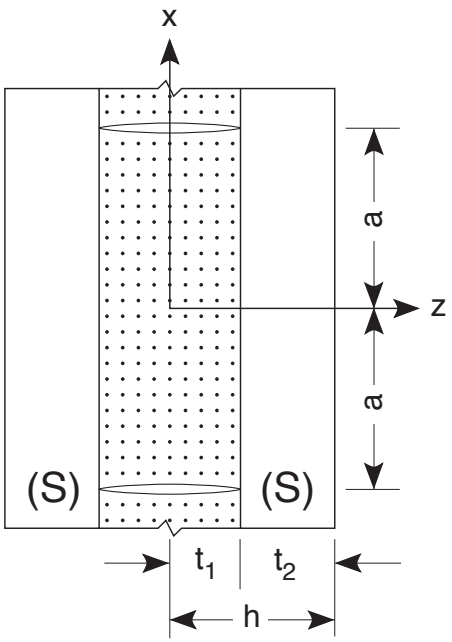

Figure 2: Edge view of a unit cell of damage between two existing straight microcracks in a $[(S)/90_n]_s$ laminate. The cracks are separated by 2a; the thickness of the $[90_n]$ sublaminate is $2t_1$; the thicknesses of the [(S)] sublaminate are t_2 each; the total laminate thickness is 2h.

explicit form of $\psi(x)$. The only assumption used in Hashin's variational analysis is that the x-axis tensile stresses in each sublaminate ($\sigma_{xx}^{(1)}$ and $\sigma_{xx}^{(2)}$) are independent of the thickness coordinate z.

Groves *et. al.*[11] first assumption states that microcracks form at locations of maximum principal stress. With the available stress state in Eq. (1), it is a simple matter to calculate the two principal stresses as a functions of x and z — $\sigma_1(x,z)$ and $\sigma_2(x,z)$. We found that the maximum principal stress, which we assigned to $\sigma_1(x,z)$ or the first principal stress, always occurs along the 0/90 interface. To predict the location of the next microcrack at the location of the maximum principal stress, we plotted the first principal stress along the interface for different straight microcrack spacings. We used a dimensionless half spacing ρ defined as

$$\rho = \frac{a}{t_1} \tag{2}$$

Typical results for various values of ρ in a $[0/90_2]_s$ carbon/epoxy laminate are given in Fig. 3. At low crack density (larger crack spacing or $\rho>2.5$) the principal stress has one maximum that is halfway between the two existing microcracks. In contrast, at high crack density (smaller crack spacing or $\rho<2.5$) the principal stress curve splits into two local maxima. There is one local maximum associated with each existing straight microcrack.

By symmetry, we infer that the principal stress trajectory halfway between two existing straight microcracks is a straight line normal to the 0/90 interface. By Groves *et. al.*[11] second

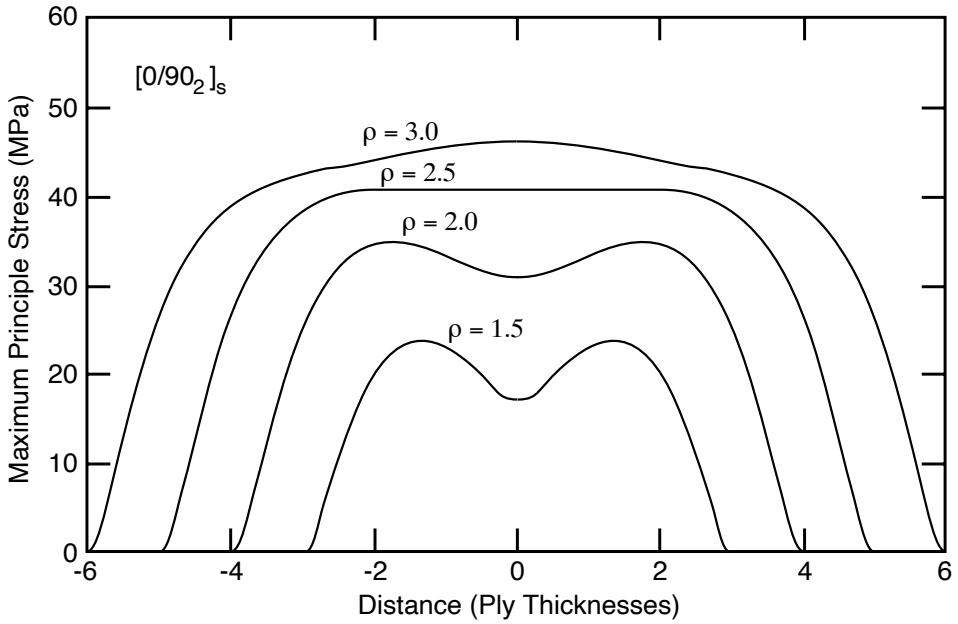

Figure 3: The first principal stress along the 0/90 interface in a typical $[0/90_2]_S$ carbon/epoxy laminate for four values of microcrack spacing. ρ is a dimensionless microcrack spacing defined by $\rho = a/t_1$. The critical value of ρ is approximately 2.5

assumption, microcracks that initiate halfway between two existing straight microcracks should develop into straight microcracks. Thus, at low crack density, cross-ply laminates tend to microcrack into an array of roughly periodic straight microcracks. This conclusion agrees with many experimental observations (*e.g.*, Refs. [1-10, 13, 14]). At high crack density, however, the maxima in principal stress occur away from the midpoint and move towards the existing straight microcracks. As discussed below, the principal stress trajectories emanating from these local stress maxima at high crack density are not straight. Thus the onset of two local principal stress maxima signals the onset of curved microcracks.

We define the critical crack density for curved microcracking as the crack density at which curved microcracks begin to form. The critical crack density can be determined by finding the crack density at which the interfacial principal stress plot makes a transition from having a single maximum halfway between two existing microcracks to having two local maxima each associated with one of the existing straight microcracks. More succinctly, the critical crack density is the density at which the equation

$$\frac{\partial \sigma_1(x,t_1)}{\partial x} = 0 \tag{3}$$

passes from having one root to having three roots. In Fig. 3, ρ=2.5 defines the critical crack spacing. For ρ>2.5, the principal stress has one maximum; for ρ<2.5, the principal stress has two

Table I: Predictions for the critical crack density for curved microcracks in AS4/PEEK composites. Also included are predictions for the location and initial angle of curved microcracks that form in a crack interval corresponding to the critical crack density.

Quantity	$[0/90_2]_s$	$[0/90_3]_s$	$[0/90_4]_s$
critical crack spacing (mm)	1.54	2.24	2.95
critical crack density (mm^{-1})	0.65	0.45	0.34
distance (mm) (x_{max})	0.521	0.667	0.790
initial angle (°) (θ)	67.8	64.0	61.4

maxima. Table I presents some theoretical predictions for critical crack densities in different layups of AS4/PEEK composites. As the number of inner 90° plies increases, the critical crack density decreases approximately linearly. Thus the thicker the 90° ply group, the sooner one can expect to see curved microcracks. This prediction agrees with experimental observations.

In opening mode (mode I) crack growth, we might expect the crack to run perpendicular to the first principal stress. The crack will then follow the trajectory of the second principal stress. By elasticity theory, the trajectory of the second principal stress is determined by the following first order differential equation:

$$\frac{dz}{dx} = -\frac{\sigma_z - \sigma_x}{2\tau_{xz}} + \sqrt{\left(\frac{\sigma_z - \sigma_x}{2\tau_{xz}}\right)^2 + 1} \tag{4}$$

where σ_1 is the first principal stress. Substituting the variational stress state in Eq. (1) we get

$$\frac{dz}{dx} = -\frac{\sigma_{x0}^{(1)} - \psi - \frac{1}{2}\psi''(ht_1 - z^2)}{2\psi' z} + \sqrt{\left(\frac{\sigma_{x0}^{(1)} - \psi - \frac{1}{2}\psi''(ht_1 - z^2)}{2\psi' z}\right)^2 + 1} \tag{5}$$

The initial angle, θ, that the curved microcrack makes with the 0/90 interface can be predicted by evaluating dz/dx at the location of the maximum in the first principal stress along the 0/90 interface. The result is

$$\tan\theta = \frac{dz(x_{max}, t_1)}{dx} \tag{6}$$

where x_{max} is the location of maximum in the first principal stress. x_{max} is determined numerically for a given crack spacing by plotting the principal stress along the 0/90 interface. The predictions of both x_{max} and the initial angle for several AS4/PEEK laminates are given in Table I. The initial

angle is always about 50-70°. It is relatively insensitive to stacking sequence and qualitatively agrees with experimental observations.

By Groves *et. al.*[11] second assumption, we can solve Eq. (5) to predict the complete shape of curved microcracks. Unfortunately, Eq. (5) is not analytically solvable. Numerical techniques, such as Euler method or Runge-Kutta method, however, can be used to obtain the relation between x and z that defines the predicted trajectory of a curved microcrack. We solved Eq. (5) using a fourth-order Runge-Kutta method. The location of maximum in the first principal stress, numerically determined earlier, was used as the initial condition. Figure 4 shows two calculated curved microcrack trajectory traced on top of two observed curved microcracks. The agreement is satisfactory. The predicted trajectories agree well with each crack at one ply interface and deviate somewhat at the other ply interface. The analysis is symmetric about the midplane and thus could never predict the asymmetry of the observed microcracks. There were no adjustable parameters in calculating the curved crack trajectories in Fig. 4. The calculation is solely a function of the size of the microcrack intervals above or below the straight microcrack. In addition, the size of the microcrack interval above the straight microcrack has no influence on the curved microcrack formation process below the straight microcrack, and *vice versa*. For the specific microcracks in Fig. 4, the observed microcrack interval above the straight crack was 5.75 mm and the interval below it was 5.5 mm.

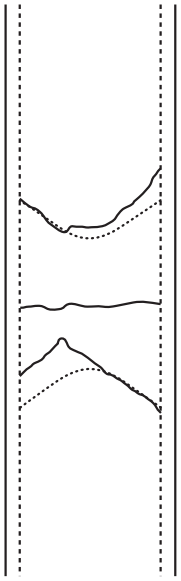

Figure 4: Predicted trajectories of two curved microcracks in a AS4/PEEK $[0/90_8]_S$ laminate compared to experimentally observed shapes. The upper experimental curved microcrack was in a microcrack interval of length 5.75 mm. The lower experimental curved microcrack was in a microcrack interval of length 5.50 mm.

We close by discussing some predictions of the theory. For the same layup, the initial angle that the curved microcrack makes with the 0/90 interface increases as the size of the microcrack interval where the curved microcrack forms increases. For the same interval size and supporting sublaminate (S), the initial angle decreases as the number of inner 90° plies increases. For the laminates studied, the distance of the maximum in the first principal stress to the existing straight microcrack, where the curved microcrack is expected to initiate, is always between one-third and one-quarter of the total spacing between the existing straight microcracks.

COMPARISON OF THEORETICAL AND EXPERIMENTAL RESULTS

For the AS4/PEEK material, we tested three laminates with inner 90° plies: $[0/90_2]_s$, $[0/90_4]_s$, $[0/90_8]_s$. Curved microcracks were observed only in the $[0/90_8]_s$ laminates. For the AS4/3501-6 material, we tested 10 laminates with inner 90° plies: $[0/90]_s$, $[0/90_2]_s$, $[0/90_4]_s$, $[0_2/90]_s$, $[0_2/90_2]_s$, $[0_2/90_4]_s$, $[\pm15/90_2]_s$, $[\pm15/90_3]_s$, $[\pm30/90_2]_s$, $[\pm30/90_3]_s$. Curved microcracks were observed only in $[\pm30/90_3]_s$, $[\pm15/90_3]_s$, $[0/90_4]_s$ laminates.

The reason that curved microcracks were observed in some laminates, but not in others, can be explained by the critical crack density for curved microcracks. To get the maximum microcrack density possible, each laminate was tested until it broke or until the end-tabs failed. For the samples that did not show curved microcracks, the maximum straight microcrack density at the end of the test was always below the critical crack density for curved microcracking. For example, the AS4/PEEK $[0/90_4]_s$ laminates did not show any curved microcracks. Among the three specimens tested, the one with maximum average straight microcrack density attained a crack density of 0.239 mm^{-1}. The calculated critical crack density for curved microcracks, however, is 0.342 mm^{-1} (see Table I). The former is lower than the predicted critical crack density required to initiate curved microcracks and this explains why these laminates and some other laminates had no curved microcracks.

Table II summarizes the experimental observations for laminates that had curved microcracks and compares them to theoretical predictions. We observed curved microcracks in four different layups and a total of eight different specimens. For each layup, we found between 3 and 14 crack intervals that had curved microcracks. The column labeled "Observed Density" gives the average microcrack density for the crack intervals having curved microcracks. Because straight microcracks never formed between existing curved microcracks, the average density for the crack intervals having curved microcracks therefore the experimentally determined critical crack density for curved microcracking. The predicted critical crack density for each laminate is given in the

Table II. Comparison of observed and predicted results for the initiation of curved microcracks in $[(S)/90_n]_s$ laminates.

Laminate	No. of Spec.	No. of Cracks	Observed Density (mm^{-1})	Predicted Density (mm^{-1})	Observed Location (mm)	Predicted Location (mm)	Predicted Angle (°)
$[\pm30/90_3]_s$*	3	14	0.362	0.422	0.928	0.850	69.9
$[\pm15/90_3]_s$*	1	5	0.500	0.418	0.760	0.905	72.4
$[0/90_4]_s$*	1	3	0.323	0.339	0.900	0.790	61.4
$[0/90_8]_s$**	3	13	0.182	0.172	1.18	1.21	56.7

* AS4/3501-6
** AS4/PEEK

column labeled “Predicted Density.” The agreement between observed and predicted densities is good. Perfect agreement was not expected because experimental microcrack density is a discrete variable that increases in a stepwise fashion following the formation of each new microcrack. Our prediction is that curved microcracks form when the microcrack density jumps past the predicted critical crack density. The stepwise increase in experimental crack density means that the predicted critical crack density defines a lower bound to the experimental result. The fact that some laminates showed curved microcracks before the predicted lower-bound critical crack density may be attributed to statistical variations in the failure processes due to laminate flaws or inhomogeneities. If there is a laminate flaw located near the 0/90 interface, that flaw may cause a premature microcrack. If the flaw happens to be near an existing straight microcrack, the principal stress trajectory will be curved resulting in initiation of a premature curved microcrack.

Table II also lists the observed locations for curved microcracks. The observed location is defined as the distance along the 0/90 interface from the existing straight microcrack to the initiation site of the curved microcrack. The agreement between the observed locations and the predicted locations is reasonable. It is noteworthy that predictions for location based on the variational analysis are considerably more accurate than similar predictions based on finite element analysis by Groves *et. al*..[11] For example, Ref. [11] describes experiments on $[0/90_2]_s$ AS4 carbon fiber/Hercules 3502 epoxy matrix composites. The experimental result for the mean distance along the 0/90 interface from the straight microcrack to the curved microcrack was 0.249 mm. The minimum distance was 0.178 mm. The average straight microcrack spacing was 0.635 mm. The finite element analysis in Ref. [11] located a peak in the principal stress near the 0/90 interface. The peak stress position, however, was 0.0508 mm from the existing microcrack. This position is much closer to the straight microcrack than the observed locations of the curved microcracks. In contrast, using the observed crack spacing of 0.635 mm and the properties of the laminates in Ref. [11], the variational analysis predicts curved microcracks to be located 0.176 mm from the straight microcrack. This analytical prediction is equal to the minimum observed crack distance and is in better agreement with experimental observation than the finite element analysis result.

The last column of Table II gives the predictions for the initial angle of curved microcracks. It was not possible to measure unambiguously the initial angle of real curved microcracks using microscopy. Our best estimates from optical microscopy and a few photographs are that the initial angles were about 60˚. This result agrees with the estimated experimental results in Ref. [11]. All experimental results qualitatively agree with the predicted angles that range from 56.7˚ to 72.4˚, with an average of 64.6˚.

DISCUSSION

Groves *et. al.*[11] propose that the initiation and orientation of curved microcracks are determined by the principal stresses. There are three observations that support their claim. First, our analytical study based on a variational analysis stress state shows that the maximum principal stresses always occur along the 0/90 interface. This calculation coincides with the experimental observation that curved microcracks initiate at the 0/90 interface. Second, both the analytical study and experimental results show that the early stages of microcracking are dominated by straight microcracks while the late stages are dominated by curved microcracking. The shift from straight microcracks to curved microcracks occurs at a critical crack density. This critical crack density can be predicted by finding the transition density at which the maximum principal stress shifts from the midpoint between two existing straight microcracks to new locations near the existing straight microcracks. The predicted critical crack density agrees with experimental results. Third, the calculated locations of the peak in the first principal stress agrees with the observed locations for curved microcracks.

In previous microcracking work,[7,14] Hashin's[6] variational analysis was used to calculate the energy release rate for the formation of a straight microcrack — G_m:

$$G_m = \left(\frac{E_{90}}{E_c}\sigma_0 - \frac{\Delta\alpha T}{C_1}\right)^2 t_1 C_3 \left(2\chi(\rho/2) - \chi(\rho)\right) \tag{7}$$

where E_{90} and E_c are the tensile moduli in the x direction of the 90° plies and the entire laminate, σ_0 is the applied stress, $\Delta\alpha = \alpha_{90} - \alpha_{(S)}$ is the difference between the x-direction thermal expansion coefficients of the 90° plies and the (S) sublaminate, T is the difference between the test temperature and the residual stress-free temperature, and C_1 and C_3 are constants defined in Refs. [6] and [7]. The function $\chi(\rho)$, which is also defined in Refs. [6] and [7], corrects the energy release rate for crack spacing, laminate properties, and laminate geometry. In Ref. [7], it was postulated that the next straight microcrack forms when the energy release rate in Eq. (7) exceeds some material property defined as the critical energy release rate for microcracking — G_{mc}. This postulate has recently been shown to agree well with many experimental observations on straight microcracking.[8, 14]

An expression analogous to Eq. (7) to give the energy release rate associated with the formation of a curved microcrack is extremely difficult to obtain. First, if we assume that the curved microcracks are complete, we might undertake an analysis of the stresses in the unit of damage in Fig. 2 following the introduction of curved microcracks near each existing straight microcrack. Unfortunately, no analytical stress state of such a damaged laminate is available. Despite some attempts, it seems unlikely that Hashin's variational analysis[6,7] is amenable to a laminate with curved microcracks. Second, experimental observations reveal that pairs of curved

microcracks that initiate at the two 0/90 interfaces may not always propagate to meet each other at the laminate midplane. The stress state of a partially microcracked medium is difficult to obtain analytically and thus it would be hard to analyze the propagation process for curved microcracks. Consequently, although the energy release rate criterion has proven useful for analysis of straight microcracks, it is not possible to derive a similar analysis for curved microcracks.

By using the maximum principal stress model, it is possible to predict the initiation of the first curved microcrack. Despite the use of principal stresses, however, we are not describing a stress criterion for failure. We are not postulating that the sample will microcrack when the maximum principal stress exceeds the strength of the material. Instead, we only assume that the *location* of the maximum principal stress defines the *location* for the initiation of the next microcrack. This assumption applies regardless of whether the next microcrack is straight or curved. We further assume that the *trajectory* of the next microcrack is determined by the *trajectory* of the second principal stress emanating from the location of the maximum in the first principal stress. When the location of the principal stress maximum is near an existing microcrack, the trajectory of the principal stress will be curved and a curved microcrack will form.

A question not previously addressed is what applied stress will cause curved microcracks to form? We answer this question indirectly from knowledge of the critical crack density for curved microcracking. Before any curved microcracks form, Eq. (7) defines the energy release rate for the formation of straight microcracks. Solving Eq. (7) for applied stress gives the predicted stress to cause the next straight microcrack. Using a single value of G_{mc} for a given material system, it is possible to predict the load required to produce a given crack density.[8,14] At the critical crack density for curved microcracking the first curved microcrack will form and Eq. (7) will cease to be valid. At the critical crack density and just before the first curved microcrack, however, Eq. (7) is still valid. Thus, the applied stress predicted by Eq. (7) to reach the critical crack density is the energy release rate prediction for the applied stress required to cause the initiation of the first curved microcrack.

Figure 4 shows that Groves *et. al.*[11] second assumption can be used, at least qualitatively, to predict the shapes of curved microcracks. This result is somewhat surprising, because once the curved microcrack initiates it perturbs the stress state and might change the principal stress trajectory. An alternative interpretation of Groves *et. al.*[11] second assumption is that the crack grows in the direction of maximum opening mode (mode I) stresses. Because the principal stress trajectory ahead of a mode I crack are collinear with the crack, the propagation of that crack might not significantly alter the original principal stress trajectory. This qualitative argument may explain why the theory can predict the final shape of curved cracks.

CONCLUSIONS

The principal stress arguments proposed by Groves *et. al.*[11] can be used along with analytical variational stress analysis to analyze the phenomenon of curved microcracking. An important finding is that curved microcracking is an unavoidable form of microcracking that occurs at high crack density. Once the microcrack density passes the critical crack density for curved microcracking, the peak principal stress shifts from halfway between two existing microcracks to along the 0/90 interface and close to the existing microcracks. Simple analyses based on principal stress criteria[11] can predict the locations for initiation of curved microcracks, their initial angles with the 0/90 interface, and their complete shapes. All predictions agree well with experimental observations. In contrast, finite element analyses[11] are more cumbersome and agree less well with experiments. The critical crack density is particularly difficult to calculate using finite element analysis because it requires multiple numerical calculations for a wide range of crack spacings for each possible laminate structure. The variational analysis can efficiently calculate the critical crack density of any $[(S)/90_n]_s$ laminate.

An important result of this work further is that it verifies the accuracy of the variational stress analysis of cross-ply laminates. References [7], [8], and [14] show that the variational analysis coupled with an energy release rate criterion can successfully predict the formation of straight microcracks. The results in this paper show that the variational analysis coupled with the principal stress assumptions[11] can predict the initiation and propagation of curved microcracks. Hashin's variational analysis is clearly a powerful tool for predicting failure of cross-ply laminates. Most alternative models for composite microcracking rely on one-dimensional or two-dimensional in-plane (x-y plane) stress analyses (*e.g.*, Refs. [1-5]). These analyses all ignore the stresses in the thickness direction—σ_{zz} and τ_{xz}. Some may include τ_{xz} but only in a manner that fails to satisfy stress equilibrium. When the z-direction stresses are ignored, the maximum principal stress is coincident with the maximum value of σ_{xx}. Because all one-dimensional analyses or two-dimensional, in-plane analyses predict that the maximum value of σ_{xx} is halfway between two existing straight microcracks, they are incapable of predicting the phenomenon of curved microcracks. They would never predict a shift in the maximum principal stress away from the midpoint between two existing straight microcracks.

We close with two litmus tests that can be used to distinguish a useful analysis of cross-ply laminates from an inadequate one. First, the analysis must be able to distinguish the microcracking properties of $[(S)/90_n]_s$ laminates from those of $[90_n/(S)]_s$ laminates. Second, the analysis must be able to predict that at a certain critical crack density the location of the maximum principal stress shifts from halfway between two existing straight microcracks to near the existing straight microcracks. Both of these litmus tests require an analysis that includes the thickness

direction stresses. Hashin's variational analysis is the only analytical analysis we know of that passes both tests (see Ref. [8]).

ACKNOWLEDGEMENTS

This work was supported in part by a contract from NASA Langley Research Center (NAS1-18833) monitored by Dr. John Crews, in part by a gift from ICI Advanced Composites monitored by Dr. J. A. Barnes, and in part by a gift from the Fibers Department of E. I. duPont deNemours & Company monitored by Dr. Alan R. Wedgewood.

REFERENCES

1. K. W. Garrett and J. E. Bailey, Multiple Transverse Fracture in 90˚ Cross-Ply Laminates of a Glass Fibre-Reinforced Polyester, *J. Mat. Sci.*, **12** (1977) pp. 157-168.
2. D. L. Flaggs, Prediction of Tensile Matrix Failure in Composite Laminates, *J. Comp. Mat.*, **19** (1985) pp. 29-50.
3. Y. M. Han, H. T. Hahn and R. B. Croman, A Simplified Analysis of Transverse Ply Cracking in Cross-Ply Laminates, *Proc. Amer. Soc. Comp., 2nd Tech. Conf.*, Newark, DE, Sept. 23-25, 1987, pp. 503-514.
4. R. J. Nuismer and S. C. Tan, Constitutive Relations of a Cracked Composite Lamina, *J. Comp. Mat.*, **22** (1988) pp. 306-321.
5. N. Law and G. Dvorak, Progressive Transverse Cracking in Composite Laminates, *J. Comp. Mat.*, **22** (1988) pp. 900-916.
6. Z. Hashin, Analysis of Cracked Laminates: A Variational Approach, *Mechanics of Materials*, **4** (1985) pp. 121-136.
7. J. A. Nairn, The Strain Energy Release Rate of Composite Microcracking: A Variational Approach, J. Comp. Mat., **23** (1989) pp. 1106-1129 (Also see *errata* published as *J. Comp. Mat.*, **24** (1990) 233).
8. J. A. Nairn and S. Hu, Micromechanics of Damage: A Case Study of Matrix Microcracking, in *Damage Mechanics of Composite Materials*, Editor R. Talreja, in press (1991).
9. K. W. Garrett and J. E. Bailey, The Effect of Resin Failure Strain on the Tensile Properties of Glass Fiber-Reinforced Cross-Ply Laminates, *J. Comp. Mat.*, **12** (1977) pp. 2189-2194.
10. A. Parvizi and J. E. Bailey, On Multiple Transverse Cracking in Glass-Fiber Epoxy Cross-Ply Laminates, *J. Mat. Sci.*, **13** (1978) pp. 2131-2136.
11. S. E. Groves, C. E. Harris, A. L. Highsmith, D. H. Allen and R. G. Norvell, An Experimental and Analytical Treatment of Matrix Cracking in Cross-Ply Laminates, *Experimental Mechanics*, March (1987) pp. 73-79.
12. D. H. Allen, C. E. Harris, S. E. Groves and R. G. Norvell, Characterization of Stiffness Loss in Cross-ply Laminates with Curved Matrix Cracks, *J. Comp. Mat.*, **22** (1988) pp. 71-80.
13. J. A. Nairn and S. Hu, The Formation and Effect of Outer-Ply Microcracks in Cross-Ply Laminates: A Variational Approach, *Eng. Fract. Mech.*, **42** (1992) pp. 203-221.
14. S. Liu and J. A. Nairn, The Formation and Propagation of Matrix Microcracks in Cross-Ply Laminates During Static Loading, *J. Reinf. Plast. & Comp.*, **11** (1992) pp. 158-178.